

The Nature of Nearby Counterparts to Intermediate Redshift Luminous Compact Blue Galaxies

II. CO Observations

C. A. Garland¹², J. P. Williams¹, D. J. Pisano³⁴⁵, R. Guzmán⁶, F. J. Castander⁷, and J. Brinkmann⁸

ABSTRACT

We present the results of a single-dish beam-matched survey of the three lowest rotational transitions of CO in a sample of 20 local ($D \lesssim 70$ Mpc) Luminous Compact Blue Galaxies (LCBGs). These $\sim L^*$, blue, high surface brightness, starbursting galaxies were selected with the same criteria used to define LCBGs at higher redshifts. Our detection rate was 70%, with those galaxies having $L_B < 7 \times 10^9 L_\odot$ not detected. We find the H_2 masses of local LCBGs range from 6.6×10^6 to $2.7 \times 10^9 M_\odot$, assuming a Galactic CO-to- H_2 conversion factor. Combining these results with our earlier H I survey of the same sample, we find that the ratio of molecular to atomic gas mass is low, typically 5 – 10%. Using a Large Velocity Gradient model, we find that the average gas conditions of the entire ISM in local LCBGs are similar to those found in the centers of star forming regions in our Galaxy, and nuclear regions of other galaxies. Star formation rates, determined from IRAS fluxes, are a few $M_\odot \text{ year}^{-1}$, much higher per unit dynamical mass than normal spirals. If this rate remains constant, the molecular hydrogen depletion time scales are short, $\sim 10 - 200$ Myr.

¹Institute for Astronomy, University of Hawai'i, 2680 Woodlawn Drive, Honolulu, HI 96822; catherine.garland@castleton.edu, jpw@ifa.hawaii.edu

²Present address: Natural Sciences Department, Castleton State College, Castleton, VT 05735

³CSIRO Australia Telescope National Facility, P.O. Box 76, Epping, NSW 1710, Australia; DJ.Pisano@csiro.au

⁴Bolton Fellow & NSF MPS Distinguished International Postdoctoral Research Fellow

⁵Present address: Naval Research Laboratory, Code 7213, 4555 Overlook Ave Sw, Washington DC 20375

⁶Department of Astronomy, University of Florida, 211 Bryant Space Science Center, P.O. Box 112055, Gainesville, FL 32611; guzman@astro.ufl.edu

⁷Institut d'Estudis Espacials De Catalunya/CSIC, Gran Capità 2-4, E-08034 Barcelona, Spain; fjc@ieec.fcr.es

⁸Apache Point Observatory, P. O. Box 59, Sunspot, NM 88349

Subject headings: galaxies: ISM — galaxies: starburst

1. Introduction

Luminous Compact Blue Galaxies (LCBGs) are a morphologically and spectroscopically diverse class of $\sim L^*$, blue, high surface brightness, high metallicity, vigorously starbursting galaxies with an underlying older stellar population (e.g. Guzmán et al. 1997). While they have small optical diameters (\sim few kpc) they are more luminous and metal-rich than the widely studied local Blue Compact Dwarf Galaxies (e.g. Thuan & Martin 1981; Taylor et al. 1994).

LCBGs are common at intermediate redshifts ($0.4 \lesssim z \lesssim 0.7$), but rare locally (Mallén-Ornelas et al. 1999). They undergo dramatic evolution, with their number density and star formation rate density decreasing by at least a factor of ten from $z \sim 1$ to today (Marzke et al. 1994; Guzmán et al. 1997). We have undertaken a survey of the neutral interstellar medium in 20 nearby ($D \lesssim 70$ Mpc) LCBGs. The galaxies are listed in Table 1 and were primarily chosen from the Sloan Digital Sky Survey (SDSS; York et al. 2000; Abazajian 2004) using a similar selection criteria to Werk et al. (2004) to be local analogs to the numerous LCBGs studied at intermediate redshifts.

In Garland et al. (2004, hereafter Paper I), we reported the results of a single-dish survey of the H I content of these galaxies and showed that LCBGs are gas-rich with velocity dispersions and optical sizes that are consistent with low-mass galaxies, despite their high luminosities. Many have disturbed morphologies and nearby companions at similar velocities. We direct the reader to Paper I for complete information on the definition of LCBGs, sample selection, optical photometric properties, and results from the H I survey.

The H I observations do not tell us, however, about the properties of the ISM that is actively forming stars. For this, it is necessary to study the molecular gas. In this work, Paper II, we report the results of a survey of the three lowest rotational transitions of CO of the same sample of 20 nearby LCBGs. CO is the most abundant, readily observable molecule in star forming clouds. The intensity of its lowest transition, 1–0, is empirically found to be a direct measure of the column density of molecular gas (Dickman 1978), and the ratio of the different transitions provides information on the temperature and density of the gas (Goldreich & Kwan 1974). The CO observations are described in §2, and the derived molecular masses, densities and temperatures are presented in §3.1-3.4. The rate at which the molecular gas forms stars is proportional to the far-infrared (IRAS) luminosity and this is discussed, along with gas depletion timescales, in §3.5. Our conclusions are listed in §4.

We assume $H_0 = 70 \text{ km s}^{-1} \text{ Mpc}^{-1}$ throughout.

2. Observations

We observed the sample of 20 nearby LCBGs in the CO(2–1) transition at the JCMT 15 m telescope and followed up clear or marginal detections with observations of CO(1–0) at the IRAM 30 m. Most of these were also observed in CO(3–2) at the CSO and HHSMT 10 m telescopes. The variety of telescopes was chosen to provide a uniform beam size, $\simeq 21''$, in each transition. The observational setup for each telescope is described below:

2.1. JCMT

The James Clerk Maxwell Telescope¹ (JCMT) was used to observe the CO(2–1) transition at 230 GHz in queue mode observations between August 2002 and January 2003. The heterodyne A3 receiver was used with the Digital Autocorrelating Spectrometer (DAS), giving a bandwidth of 920 MHz ($\sim 1200 \text{ km s}^{-1}$). System temperatures ranged from 400 to 600 K and sources were typically observed until the rms noise per 10 km s^{-1} channel was 10 mK, or the peak signal-to-noise was greater than five.

2.2. IRAM

The Institut de Radioastronomie Millimétrique (IRAM) 30 m Telescope was used to observe the CO(1–0) transition at 115 GHz between August 2001 and October 2003 using the A100 and B100 heterodyne receivers. The 1 MHz filterbank was split in half giving a bandwidth of 512 MHz ($\sim 1300 \text{ km s}^{-1}$) in 2003 October, and was split in four giving a bandwidth of 256 MHz ($\sim 670 \text{ km s}^{-1}$) in 2002 May and 2001 August. System temperatures averaged 500 K and sources were typically observed until the noise was 5 mK per 10 km s^{-1} channel, or a peak signal-to-noise greater than five was reached.

The CO(2–1) transition was observed simultaneously with the A230 and B230 receivers. The autocorrelator backend was configured to a bandwidth of 320 MHz ($\sim 415 \text{ km s}^{-1}$) per receiver. The resolution of these data is $11''$.

¹The JCMT is operated by the Joint Astronomy Centre in Hilo, Hawai'i on behalf of the parent organizations Particle Physics and Astronomy Research Council in the United Kingdom, the National Research Council of Canada and The Netherlands Organization for Scientific Research.

2.3. HHSMT

Observations of CO(3–2) were performed with the Heinrich Hertz Sub-Millimeter Telescope (HHSMT) in February 2002. Mrk 297, Mrk 325 and SDSSJ0934+0014 were observed using the double sideband dual channel SIS-345 GHz heterodyne receiver B30/B40, each with a 1 GHz ($\sim 870 \text{ km s}^{-1}$) Acousto-Optical-Spectrometer (AOS) backend. System temperatures ranged from 700 to 800 K.

2.4. CSO

Two observing runs in March and July 2003 with the Caltech Submillimeter Observatory (CSO) completed the CO(3–2) observations listed in Table 2. The 345 GHz heterodyne receiver and 1.5 GHz ($\sim 1300 \text{ km s}^{-1}$) AOS backend were used. System temperatures averaged 700 K and sources were typically observed until the rms noise was $\sim 10 \text{ mK}$ per 10 km s^{-1} channel, or the peak signal-to-noise was greater than five.

For each telescope, the observations were performed in beam-switching mode with a throw of $240''$ and rate between 0.5 and 1 Hz. System temperature calibrations were taken roughly every 20 minutes, as well as each time a new source was observed. Pointing and main beam calibration scans were done on planets or bright carbon stars at least once every three hours. The focus was checked several times each night, particularly near sunrise and sunset.

2.5. Reduction and Calibration

All data were reduced in a similar manner, using the Continuum and Line Analysis Single-dish Software (CLASS) for the IRAM, HHT and CSO data, while the JCMT data were reduced using SPECX. A first or second order baseline was removed from each scan, avoiding the region of line emission. If no emission line was obvious in the scan, a region of at least $\pm 50 \text{ km s}^{-1}$ from the optical velocity was avoided. The individual scans were then combined, and a first order baseline removed. Spectra were converted to the heliocentric velocity scale, using the optical convention, and smoothed to a common resolution of $\sim 10 \text{ km s}^{-1}$, using a boxcar smoothing routine. The IRAM data for Mrk 297 are from Sage et al. (1993) and were digitized from plots kindly provided by Leslie Sage.

The data were calibrated from raw intensity to the scale of corrected antenna temperature (T_A^*) at each telescope using the conventional “chopper wheel method” where loads

are measured at ambient and cold temperatures. The spectra were then calibrated from this telescope dependent quantity to main beam temperature (T_{mb}). Both IRAM and JCMT maintain web-based databases of main beam efficiencies, η_{mb} , which we used for calibration. For the IRAM data, $\eta_{mb} = 0.79$ for the 115 GHz data, and $\eta_{mb} = 0.57$ for the 230 GHz data. The JCMT main beam efficiencies ranged from $\eta_{mb} = 0.55$ to 0.71 depending on the month of observation. The HHT spectra were calibrated by comparing observations of IRC+10216 with the spectral line survey of Groesbeck et al. (1994), as well as by observations of Mars. We used $\eta_{mb} = 0.59$ for receiver B30 and $\eta_{mb} = 0.48$ for receiver B40. We also calibrated the CSO data using observations of IRC+10216, finding $\eta_{mb} = 0.60$.

3. Results

3.1. Line measurements and detectability

The CO spectra are shown in Figures 1, 2, 3, and 4. Each galaxy’s velocity, calculated from the optical redshift, is indicated with a triangle. The galaxies exhibit a variety of spectra, including Gaussian, double-horned and asymmetric profiles. Line measurements, calculated by taking moments of the spectra, are listed in Table 2. We list the mean (heliocentric) velocity, V_{\odot} , and dispersion, σ , from the CO(1–0) observations, except where noted. In general, the central velocities and line widths agree well from transition to transition but the higher CO transitions tend to have slightly smaller line widths. This may be due to the central concentration of the warmer, denser gas. The CO velocity dispersions were always found to be smaller than the H I velocity dispersions calculated in the same manner (Paper I).

For those spectra with no discernible emission line, we calculated 3σ upper limits to the integrated intensity, I_{CO} , over the average number of channels containing CO emission for that transition and beam size combination. Blank entries in Table 2 indicate the source was not observed with that transition and beam size combination. The uncertainties on I_{CO} were calculated from the measured noise in the channels outside of the emission line region. The uncertainties on the recessional velocities and line widths were estimated by creating 1000 simulated spectra from each observed spectrum, and measuring the dispersion of the calculated recessional velocities and line widths.

Six galaxies, SDSSJ0119+1452, SDSSJ0218–0757, SDSSJ0222–0830, SDSSJ0728+3532, SDSSJ0834+0139, and SDSSJ1319+5203 were not detected in CO above the 3σ level. We do not expect that beam dilution is a serious problem because the typical optical diameter, D_{25} (Table 1), is roughly twice the uniform 21" resolution of the data. Young et al. (1995)

found that CO extends over half the optical disk, on average, in a sample of over 300 nearby galaxies of varied Hubble types and environments and therefore we expect the telescope beam sizes enclose most of the CO emission for most of our sample. We did find that the detection rate was lower for the smallest galaxies, those with $R_{25} \lesssim 21''$. Regardless of size, all galaxies with luminosities, $L_B > 7 \times 10^9 L_\odot$ ($M_B < -19.1$) were detected.

3.2. Molecular Masses

We converted the CO integrated intensities to molecular hydrogen masses using a Galactic conversion factor of $1.8 \times 10^{20} \text{ cm}^{-2} \text{ K}^{-1} \text{ km}^{-1} \text{ s}$ (Dame et al. 2001). This “X” factor, is only well calibrated for the Milky Way and Local Group. It depends on the physical conditions of the gas (e.g. metallicity, density, temperature) which are difficult to determine and may differ greatly from those in our own Galaxy (Taylor et al. 1998; Sage et al. 1992). There is considerable debate over how X depends on galaxy properties, particularly in low metallicity and/or starbursting galaxies (e.g., Wilson 1995; Yao et al. 2003) and also, interestingly, resolution (Rosolowsky et al. 2003). The consensus from the latest studies is that X is not as sensitive to metallicity as older lower resolution measurements had suggested.

We also expect local LCBGs to have near-solar metallicities based on observations of intermediate redshift LCBGs (Guzmán et al. 1996; Kobulnicky & Koo 2000), and the four local LCBGs for which there are metallicity estimates in the literature (Calzetti 1997; Hunter & Gallagher 1986). Based on this and the lack of any clear dependence of X on metallicity, we adopt the Galactic value for converting our measured CO intensities to molecular masses.

The empirical relation for the mass of H_2 is calibrated for the CO(1–0) transition. We have observed 14 galaxies in CO(1–0), and detected 12 of those. The two non-detections, Mrk 314 and SDSSJ0834+0139, are treated differently: Mrk 314 was detected in CO(2–1) with the larger collecting area and smaller beam, $11''$, of the IRAM 30 m and we use the integrated intensity of that spectrum to convert to a column density and then mass. SDSSJ0834+0139 was undetected even at higher resolution and we use the 3σ upper limit from the CO(1–0) observations. For the galaxies not observed in CO(1–0) at IRAM, we used the CO(2–1) $\theta = 21''$ observations, either 3σ upper limits or detections from the JCMT data. It is reasonable to estimate the H_2 mass using CO(2–1) instead of CO(1–0) as we find the ratio of these integrated intensities is 1.1 ± 0.21 .

The H_2 masses of local LCBGs are listed in Table 2 and range from 6.6×10^6 to $2.7 \times 10^9 M_\odot$, with a median of $1.8 \times 10^8 M_\odot$ (including upper limits). Molecular hydrogen masses range from less than 1×10^6 to $5 \times 10^{10} M_\odot$ across the range of galaxy types (Young

& Scoville 1991), so LCBGs are not extreme in either direction. The most massive LCBGs have molecular masses comparable to the Milky Way but the average is an order of magnitude smaller. We also note that the H_2 masses are all less than the upper limits in $z \sim 0.5$ LCBGs obtained by Wilson & Combes (1998).

3.3. Comparison with HI observations

It is instructive to compare these observations of the molecular ISM with the observations of the neutral atomic ISM in Paper I. CO and HI spectra are plotted for each of the 20 galaxies in our sample in Figure 5. The CO spectra are generally the 1–0 transition from the IRAM 30 m observations (21'' resolution) except for Mrk 314, which was only detected in the 2–1 transition (at 11'' resolution), and the six galaxies, SDSSJ0119, 0218, 0222, 0728, 1319 and 1507 which were not observed with IRAM, and where we show the JCMT CO(2–1) spectra (21'' resolution) instead. The HI spectra were taken with the Green Bank Telescope (GBT; 9' resolution) and are discussed in more detail in Paper I. For ease of comparison, the galaxies are ordered from highest blue luminosity to lowest and are shown over the same velocity width, 650 km s^{-1} . The temperature/flux density scale is also the same for all but five galaxies, indicated by asterisks in the title to each panel, where the spectra are scaled down by a factor of four.

The HI spectra generally have a much higher signal-to-noise ratio than the CO but, nevertheless, it is clear that the CO-to-HI ratio varies greatly across our sample. In Figure 6 we plot the mass of molecular versus atomic hydrogen for the 14 LCBGs detected in CO. The ratio of molecular to atomic gas masses is low, typically $\lesssim 10\%$. Young & Knezek (1989) showed that the mean molecular to atomic mass fraction varied systematically along the Hubble sequence from 2.6 ± 1.2 for type S0/Sa to 0.12 ± 0.064 for type Sd/Sm (for $X = 1.8 \times 10^{20} \text{ cm}^{-2} \text{ K}^{-1} \text{ km}^{-1} \text{ s}$.) LCBGs have a mean $M(H_2)$ to $M(H I)$ ratio of 0.05 ± 0.002 , even smaller than the median for late-type local spirals. Within our LCBG sample, however, we were unable to find a correlation between a galaxy's morphology in the SDSS optical images and its molecular-to-atomic mass ratio.

Young & Knezek (1989) found that it is the phase, not the amount, of neutral gas that changes with Hubble type. They argue that the bulk of the decrease in the ratio of $M(H_2)$ to $M(H I)$ with Hubble type is from different surface densities of the gas in the inner disks of early versus late-type spirals. Blitz & Rosolowsky (2004) hypothesize that the hydrostatic pressure, set by the *stellar* surface density, determines how much of the ISM is molecular or atomic at each radius. There is some support for these ideas in the weak correlation between the molecular to atomic mass fraction and dynamical mass, shown in Figure 7.

3.4. H₂ densities and temperatures

Comparing the integrated intensities of different CO transitions observed with the same beam size allows us to probe the excitation conditions in the molecular gas. As we are dealing with single-dish unresolved observations, our findings are for the *average* conditions in the molecular gas in the galaxies. We list the observed line ratios in Table 3, defined as

$$\mathcal{R}_{ij} = \frac{I_{CO}(i \rightarrow i-1)}{I_{CO}(j \rightarrow j-1)},$$

for $(i, j) = (3, 1), (3, 2)$ and $(2, 1)$.

The noise in the JCMT CO(2–1) spectrum of Mrk 325 was quite high, leading to large uncertainties in the line ratios. While observing Mrk 325 with the IRAM 30 m, we did a five point map of the galaxy, with observations spaced by $\pm 10''$ from the central galaxy position. Using a weighted sum, we created a 2–1 spectrum to mimic a $21''$ beam. We found that this spectrum of Mrk 325 matched the JCMT CO(2–1) $\theta = 21''$ spectrum, but with significantly better signal-to-noise. Therefore, we utilized the values from the IRAM CO(2–1) observations of Mrk 325 in our line ratio analysis.

In the sample of local LCBGs, \mathcal{R}_{21} ranges from 0.83 to 1.6, with a mean of 1.1 ± 0.21 . Our observations are in good agreement with those of Aalto et al. (1995) who found $\langle \mathcal{R}_{21} \rangle = 0.93 \pm 0.22$ in a study of a variety of infrared-bright galaxies. Note, however, that their observations only cover the central positions of the galaxies. Optically thick CO emission arising from thermalized gas at $T > 10$ K yields $\mathcal{R}_{21} \sim 1$ assuming a homogeneous source characterized by a single temperature and density (Bolatto et al. 2003). Ratios lower than unity can be caused by low temperature or volume density or departures from homogeneity. For example, $\langle \mathcal{R}_{21} \rangle = 0.5$ in the Taurus Dark Cloud with slightly higher values $\mathcal{R}_{21} \gtrsim 0.7$ found in Giant Molecular Clouds, such as Orion A (Hasegawa 1996; Kunth et al. 1996).

We find \mathcal{R}_{31} ranges from 0.24 to 1.2, with a mean of 0.72 ± 0.33 , in the local sample of LCBGs. Yao et al. (2003) studied the central regions of 60 infrared luminous galaxies and found \mathcal{R}_{31} to range from 0.22 to 1.72, with a median of 0.66. These findings are similar to a study by Mauersberger et al. (1999) who found \mathcal{R}_{31} to range from 0.1 to 1.6, with a median of 0.63, in a sample of nearby spiral galaxies. They note that, as many of their galaxies are extended with respect to the beam, their findings may reflect conditions in the nuclear region. Meier et al. (2001) found \mathcal{R}_{31} to range from 0.37 to 1.1, with a median of 0.61 ± 0.06 in a sample of dwarf (low luminosity) starburst galaxies. These median values are larger than the average over a Milky Way giant molecular cloud ($\mathcal{R}_{31} = 0.4$) but similar to the denser clumps within it ($\mathcal{R}_{31} = 0.6 - 1$) (Williams & Blitz 1998; Sanders et al. 1993). That is, the *average* conditions of the entire molecular ISM in our LCBGs are similar to the

conditions found in the *cores* of star forming regions in our own Galaxy and the *centers* of other galaxies.

We can further constrain the physical conditions of the molecular gas using a Large Velocity Gradient (LVG; Goldreich & Kwan 1974) model for the eight galaxies detected in all three transitions of CO. In the models, we utilized an inferred column density of CO, N_{CO} , assuming a CO abundance of 10^{-4} relative to H_2 (Hollenbach & Tielens 1999), and CO-to- H_2 conversion factor of $1.8 \times 10^{20} \text{ cm}^{-2} \text{ K}^{-1} \text{ km}^{-1} \text{ s}$ (Table 4). We ran the models for a grid of kinetic temperatures, T_K , between 5 and 200 K, and volume densities, $n(H_2)$, between 10 and 10^7 cm^{-3} . We then derived model intensity ratios, \mathcal{R}_{21} , \mathcal{R}_{31} and \mathcal{R}_{32} and searched for temperature and density combinations that matched the corresponding three observed values.

The results of our LVG modeling of six LCBGs are shown in Figure 8. We were able to fit all three ratios within $\pm 1\sigma$ in three cases, Mrk 297, Mrk 538, and SDSSJ0911+4638. A wide variety of temperature and density combinations were found, however, ranging from $T = 10$ to 150 K, and $n(H_2) \lesssim 10^3$ to $2 \times 10^4 \text{ cm}^{-3}$. Our findings are similar to the study of dwarf starburst galaxies by Meier et al. (2001).

For three other galaxies, SDSSJ0904+5136, SDSSJ0934+0014, and SDSSJ2317+1400, we found fits that matched the ratios within $\pm 3\sigma$, but these only provided lower temperature limits and upper density limits. We were unable to find any combinations of temperature and volume density which worked simultaneously for all three line ratios for the remaining two galaxies, Mrk 325 and SDSSJ0943–0215. The temperatures and densities which match \mathcal{R}_{21} and \mathcal{R}_{31} are inconsistent with those for \mathcal{R}_{32} , even at very high temperatures ($> 200 \text{ K}$) and volume densities ($> 10^5 \text{ cm}^{-3}$). To produce a fit in these galaxies, we would need to increase N_{CO} above the observed values of $\sim 5 \times 10^{16} \text{ cm}^{-2}$, by approximately an order of magnitude. Note that our findings would change if we utilized different values of N_{CO} . For example, if the X factor or the CO to H_2 abundance were higher, then the inferred N_{CO} would be larger, and lower temperatures and/or densities would be predicted.

3.5. Star Formation Rates and Gas Depletion Time Scales

We extracted InfraRed Astronomical Satellite (IRAS) fluxes at 12, 25, 60 and $100 \mu\text{m}$ from the Faint Source Catalog v2.0 (FSC) for all but one source, SDSSJ0222–0830, which was not cataloged. Table 1 lists the infrared luminosities, estimated from the 60 and $100 \mu\text{m}$ fluxes based on the formulation of Kewley et al. (2002). Five galaxies in our sample have companions within $5'$ (Table 1) and may be confused at $100 \mu\text{m}$. The effect is likely to be

minor: for example, Mrk 538 is resolved in the IRAS High Resolution Image Restoration (HIRES) Atlas of Surace et al. (2004) but the 60 and 100 μm fluxes of the primary vary by less than 10% from those in the FSC.

We used the infrared luminosities derived from the FSC fluxes to calculate star formation rates (SFRs) following Kennicutt et al. (1994). Note that these SFRs assume that young stars dominate the radiation field in the ultraviolet to visible range (Kewley et al. 2002). This is a reasonable assumption for starbursting galaxies such as LCBGs. For example, Rosa-González et al. (2002) showed consistency between SFRs derived from $\text{H}\alpha$ and IRAS fluxes for a sample of 31 nearby star forming galaxies, such as H II galaxies, starburst galaxies, and blue compact galaxies. As a check, we also derived SFRs from the 1.4 GHz radio continuum for the 15 LCBGs cataloged in the National Radio Astronomy Observatory Very Large Array Sky Survey (NVSS; Condon et al. 1998) using the prescription of Bell (2003) and found excellent agreement with the infrared estimates. The correlation between radio continuum and far-infrared fluxes is well established for all galaxy types (Condon 1992) and it is reassuring to see that LCBGs are not an exception to this relation.

The SFRs range from 0.4 to 14 $M_{\odot} \text{ year}^{-1}$, with a median of 1.5 $M_{\odot} \text{ year}^{-1}$ (Table 1) for our sample of local LCBGs. This is comparable to values measured for intermediate redshift ($0.2 \lesssim z \lesssim 1$) LCBGs from [O II] equivalent widths (Guzmán et al. 1997). LCBGs have similar far infrared luminosities and SFRs to more massive local, normal spiral galaxies (Roberts & Haynes 1994). The *specific* star formation rates (SSFR), defined as the ratio of SFR to dynamical mass (Guzmán et al. 1997), is therefore considerably enhanced in LCBGs. Local LCBGs have SSFRs, calculated using the dynamical mass within $R_e(\text{B})$ (Paper I), ranging from 1.1 to $6.6 \times 10^{-10} \text{ year}^{-1}$. These SSFRs are much higher than those measured for quiescent early-type spirals, $< 10^{-11} \text{ year}^{-1}$. They are more similar to H II galaxies, which have SSFRs ranging from 1.3×10^{-10} to $4.1 \times 10^{-9} \text{ year}^{-1}$, and intermediate redshift ($0.2 \lesssim z \lesssim 1$) LCBGs, with SSFRs between 2×10^{-11} to $1.3 \times 10^{-9} \text{ year}^{-1}$ (Guzmán et al. 1997).

Determining how long a LCBG can continue to form stars at its current rate provides a direct constraint on its evolutionary possibilities. We can estimate how long a starburst will last by calculating the gas depletion time scale, $\tau_{gas} = M_{gas}/SFR$. In local LCBGs, the molecular gas depletion time scales, $\tau(\text{H}_2)$, range from 10 to 200 Myr (Table 2). The total gas depletion time may be as much as a factor of 20 times longer because the molecular mass fraction is only ~ 0.05 , but this requires efficient conversion of atomic to molecular gas. Even so, most LCBGs have gas depletion timescales that are much shorter than the lookback time to their period of greatest number density at $z \sim 1$ and we therefore expect most of them to fade and redden as they evolve into other galaxy types.

An alternate way of representing gas depletion time scales is in terms of infrared and CO luminosities (L_{IR} and L_{CO} ; Solomon et al. 1997). These are plotted against each other in Figure 9 for our sample of local LCBGs and compared to isolated galaxies, interacting local spirals, and UltraLuminous InfraRed Galaxies (ULIRGs) using values from Solomon et al. (1997) and Solomon & Sage (1988). The gas depletion time scale, proportional to L_{CO}/L_{IR} , is shorter in LCBGs than in most isolated or weakly-interacting spirals, but are similar to strongly-interacting spirals and ULIRGs. LCBGs resemble scaled-down ULIRGs, in the sense that they have high L_{IR} to L_{CO} ratios, but lower luminosities. It is thought that the star formation efficiency is high, or the gas depletion time scale is short, in perturbed environments because colliding gas flows can lead to high compression of gas (e.g. Sofue et al. 1993). Inspection of the SDSS optical images, however, shows no obvious pattern between how disturbed a galaxy appears and its location in this plot.

Nevertheless, based on Figure 9, can we consider LCBGs to be simply miniature versions of (ultra-)luminous infrared and interacting galaxies? If so, we would expect them to produce most of their luminosity in the far-infrared. Spectral energy distributions for the local LCBG sample are shown and compared with a normal spiral, NGC 2967, and prototypical ULIRG, Arp 220, in Figure 10. About equal proportions of the total energy of an LCBG is produced in the far-infrared as in the optical. This is more than for normal spirals but far less than the dramatic infrared excesses found in strongly interacting galaxies or ULIRGs (e.g. Sanders & Mirabel 1996). This difference in the SEDs between ULIRGs and LCBGs cannot be accounted for by lower metallicities or dust content in the latter as only a small amount of dust is required to reprocess short wavelength light to the far-infrared. Thus the locations of LCBGs in Figure 9, and the inferred short gas depletion timescales, are due not only to the high specific star formation rates but also a limited molecular gas reservoir.

4. Conclusions

We have observed a sample of 20 local LCBGs in the three lowest rotational transitions of CO. 14 galaxies were detected, including all with blue luminosities $L_B > 7 \times 10^9 L_\odot$. Using a Galactic conversion factor between CO intensity and H_2 column density, we find H_2 masses ranging from 6.6×10^6 to $2.7 \times 10^9 M_\odot$ with a median of $1.8 \times 10^8 M_\odot$, including upper limits. The molecular to atomic hydrogen mass fraction is low, typically $\lesssim 10\%$, which may be due to the shallow gravitational potential of these galaxies.

The line ratios of the three lowest CO transitions are similar to those found in other low mass star bursting galaxies. Using an LVG model, we find that the *average* gas conditions in local LCBGs are similar to those found in star forming regions in our Galaxy, and nuclear

regions of other galaxies.

Star formation rates, inferred from IRAS fluxes, range from 0.4 to 14 M_{\odot} year⁻¹ with a median of 1.5 M_{\odot} year⁻¹. When normalized by dynamical mass (i.e., the specific star formation rate), this is much larger than normal spiral galaxies. If stars form at a constant rate, the molecular gas will be used up in 10 – 200 Myr, similar to depletion timescales in ULIRGs and local strongly-interacting spirals. We emphasise that nearly half the local sample of local LCBGs have optical companions at similar velocities (Paper I). Many have disturbed morphologies and some are actively interacting. It is likely that interactions are even more common for the higher redshift sample because of the higher space density of galaxies (Ellis et al. 2000). Understanding the possible end-states resulting from such mergers requires higher resolution (interferometric) observations and is the subject of a future paper.

We thank Phil Solomon for encouraging us to compare our results with his ULIRG studies, Dave Sanders and Bob Joseph for helpful discussions about SEDs and SFRs, and Leslie Sage for providing copies of his CO observations of Mrk 297. We also thank Harold Butner, Baltasar Vila-Vilaro, Hervé Aussel, Axel Weiss, and the staff at the IRAM 30 m, JCMT and CSO for their help with the observations and data calibration. D. J. P. acknowledges generous support from NSF MPS Distinguished Research Fellowship grant AST-0104439.

Funding for the creation and distribution of the SDSS Archive has been provided by the Alfred P. Sloan Foundation, the Participating Institutions, the National Aeronautics and Space Administration, the National Science Foundation, the U.S. Department of Energy, the Japanese Monbukagakusho, and the Max Planck Society. The SDSS Web site is <http://www.sdss.org/>. The SDSS is managed by the Astrophysical Research Consortium (ARC) for the Participating Institutions. The Participating Institutions are The University of Chicago, Fermilab, the Institute for Advanced Study, the Japan Participation Group, The Johns Hopkins University, Los Alamos National Laboratory, the Max-Planck-Institute for Astronomy (MPIA), the Max-Planck-Institute for Astrophysics (MPA), New Mexico State University, University of Pittsburgh, Princeton University, the United States Naval Observatory, and the University of Washington. This research has also made use of the NASA/IPAC Infrared Science Archive, which is operated by the Jet Propulsion Laboratory, California Institute of Technology, under contract with the National Aeronautics and Space Administration. We have made use of the NASA/IPAC Extragalactic Database (NED) which is operated by the Jet Propulsion Laboratory, California Institute of Technology, under contract with NASA (<http://nedwww.ipac.caltech.edu/>).

REFERENCES

- Aalto, S., Booth, R. S., Black, J. H., & Johansson, L. E. B. 1995, *A&A*, 300, 369
- Abazajian, K. e. a. 2004, *AJ*, 128, 502
- Bell, E. F. 2003, *ApJ*, 586, 794
- Bolatto, A. D., Leroy, A., Israel, F. P., & Jackson, J. M. 2003, *ApJ*, 595, 167
- Calzetti, D. 1997, *AJ*, 113, 162
- Condon, J. J. 1992, *ARA&A*, 30, 575
- Condon, J. J., Cotton, W. D., Greisen, E. W., Yin, Q. F., Perley, R. A., Taylor, G. B., & Broderick, J. J. 1998, *AJ*, 115, 1693
- Dame, T. M., Hartmann, D., & Thaddeus, P. 2001, *ApJ*, 547, 792
- Dickman, R. L. 1978, *ApJS*, 37, 407
- Ellis, R. S., Abraham, R. G., Brinchmann, J., & Menanteau, F. 2000, *Astronomy and Geophysics*, 41, 10
- Garland, C. A., Pisano, D. J., Williams, J. P., Guzmán, R., & Castander, F. J. 2004, *ApJ*, 615, 689
- Goldreich, P. & Kwan, J. 1974, *ApJ*, 189, 441
- Groesbeck, T. D., Phillips, T. G., & Blake, G. A. 1994, *ApJS*, 94, 147
- Guzmán, R., Gallego, J., Koo, D. C., Phillips, A. C., Lowenthal, J. D., Faber, S. M., Illingworth, G. D., & Vogt, N. P. 1997, *ApJ*, 489, 559
- Guzmán, R., Koo, D. C., Faber, S. M., Illingworth, G. D., Takamiya, M., Kron, R. G., & Bershad, M. A. 1996, *ApJ*, 460, L5
- Hasegawa, T. 1996, in *IAU Symp. 170: CO: Twenty-Five Years of Millimeter-Wave Spectroscopy*, 39
- Hollenbach, D. J. & Tielens, A. G. G. M. 1999, *Reviews of Modern Physics*, 71, 173
- Hunter, D. A. & Gallagher, J. S. 1986, *PASP*, 98, 5
- Kennicutt, R. C., Tamblyn, P., & Congdon, C. E. 1994, *ApJ*, 435, 22

- Kewley, L. J., Geller, M. J., Jansen, R. A., & Dopita, M. A. 2002, *AJ*, 124, 3135
- Kobulnicky, H. A. & Koo, D. C. 2000, *ApJ*, 545, 712
- Kunth, D., Guiderdoni, B., Heydari-Malayeri, M., & Thuan, T. X., eds. 1996, *The interplay between massive star formation, the ISM and galaxy evolution*
- Mallén-Ornelas, G., Lilly, S. J., Crampton, D., & Schade, D. 1999, *ApJ*, 518, L83
- Marzke, R. O., Geller, M. J., Huchra, J. P., & Corwin, H. G. 1994, *AJ*, 108, 437
- Mauersberger, R., Henkel, C., Walsh, W., & Schulz, A. 1999, *A&A*, 341, 256
- Meier, D. S., Turner, J. L., Crosthwaite, L. P., & Beck, S. C. 2001, *AJ*, 121, 740
- Roberts, M. S. & Haynes, M. P. 1994, *ARA&A*, 32, 115
- Rosa-González, D., Terlevich, E., & Terlevich, R. 2002, *MNRAS*, 332, 283
- Rosolowsky, E., Engargiola, G., Plambeck, R., & Blitz, L. 2003, *ApJ*, 599, 258
- Sage, L. J., Loose, H. H., & Salzer, J. J. 1993, *A&A*, 273, 6
- Sage, L. J., Salzer, J. J., Loose, H.-H., & Henkel, C. 1992, *A&A*, 265, 19
- Sanders, D. B. & Mirabel, I. F. 1996, *ARA&A*, 34, 749
- Sanders, D. B., Scoville, N. Z., Tilanus, R. P. J., Wang, Z., & Zhou, S. 1993, in *AIP Conf. Proc. 278: Back to the Galaxy*, 311
- Sofue, Y., Wakamatsu, K., Taniguchi, Y., & Nakai, N. 1993, *PASJ*, 45, 43
- Solomon, P. M., Downes, D., Radford, S. J. E., & Barrett, J. W. 1997, *ApJ*, 478, 144
- Solomon, P. M. & Sage, L. J. 1988, *ApJ*, 334, 613
- Surace et al. 2004, *AJ*, submitted
- Taylor, C. L., Brinks, E., Pogge, R. W., & Skillman, E. D. 1994, *AJ*, 107, 971
- Taylor, C. L., Kobulnicky, H. A., & Skillman, E. D. 1998, *AJ*, 116, 2746
- Thuan, T. X. & Martin, G. E. 1981, *ApJ*, 247, 823
- Werk, J. K., Jangren, A., & Salzer, J. J. 2004, *ApJ*, 617, 1004
- Williams, J. P. & Blitz, L. 1998, *ApJ*, 494, 657

Wilson, C. D. 1995, ApJ, 448, L97

Wilson, C. D. & Combes, F. 1998, A&A, 330, 63

Yao, L., Seaquist, E. R., Kuno, N., & Dunne, L. 2003, ApJ, 588, 771

York et al., D. G. 2000, AJ, 120, 1579

Young, J. S. & Knezek, P. M. 1989, ApJ, 347, L55

Young, J. S. & Scoville, N. Z. 1991, ARA&A, 29, 581

Young, J. S., Xie, S., Tacconi, L., Knezek, P., Viscuso, P., Tacconi-Garman, L., Scoville, N., Schneider, S., Schloerb, F. P., Lord, S., Lesser, A., Kenney, J., Huang, Y., Devereux, N., Claussen, M., Case, J., Carpenter, J., Berry, M., & Allen, L. 1995, ApJS, 98, 219

Table 1. Properties of local LCBG Sample

Source	D_{OPT}^a (Mpc)	D_{25}^b (arc sec)	L_B^c ($10^9 L_{B\odot}$)	L_{IR} ($10^9 L_{\odot}$)	SFR ($M_{\odot} \text{ year}^{-1}$)	Companions within 5'
Mrk 297	67	49	39	47	14	merger
Mrk 314	30	52	3.9	1.6	0.50	
Mrk 325	49	90	16	18	5.5	
Mrk 538	40	114	17	24	7.3	✓
SDSS J011932.95+145219.0	59	40	5.6	3.7	1.1	
SDSS J021808.75–075718.0	69	29	5.2	2.4	0.74	
SDSS J022211.96–083036.2	67	26	4.3			
SDSS J072849.75+353255.2	56	40	5.6	3.4	1.0	
SDSS J083431.70+013957.9	59	44	6.8	6.5	2.0	✓
SDSS J090433.53+513651.1	68	44	12	8.5	2.6	
SDSS J091139.74+463823.0	61	38	8.2	5.1	1.5	
SDSS J093410.52+001430.2	70	41	13	22	6.8	✓
SDSS J093635.36+010659.8	71	42	6.8	4.4	1.3	✓
SDSS J094302.60–021508.9	68	29	8.2	6.1	1.8	
SDSS J111836.35+631650.4	46	28	4.3	1.3	0.38	
SDSS J123440.89+031925.1	67	42	7.4	4.9	1.5	
SDSS J131949.93+520341.1	67	33	4.7	3.7	1.10	✓
SDSS J140203.52+095545.6	61	59	12	16	4.7	
SDSS J150748.33+551108.6	48	67	5.6	1.4	0.42	
SDSS J231736.39+140004.3	63	48	8.2	11	3.4	

^a Distance from optical redshifts, see Paper I.

^b Isophotal diameter at the limiting surface brightness of 25 B-magnitudes arc sec⁻², from NED.

^c From Paper I.

Table 2. CO Line Measurements and Derived Properties

Source	V_{\odot}	σ	I_{CO} (J=1-0) $\theta = 21''$	I_{CO} (J=2-1) $\theta = 11''$	I_{CO} (J=2-1) $\theta = 21''$	I_{CO} (J=3-2) $\theta = 21''$	M(H ₂)	τ (H ₂)
	(km s ⁻¹)	(km s ⁻¹)	(K km s ⁻¹)	(K km s ⁻¹)	(K km s ⁻¹)	(K km s ⁻¹)	(10 ⁸ M _⊙)	(10 ⁶ years)
Mrk 297	4728 ± 2	49 ± 1	24 ± 0.63	29 ± 0.84	20 ± 0.38	5.7 ± 0.79	27 ± 0.7	193
Mrk 314	2105 ± 4 ^a	37 ± 2 ^a	< 0.33	1.2 ± 0.11	< 1.0		0.066 ± 0.0061	13
Mrk 325	3423 ± 1	22 ± 1	2.8 ± 0.081	4.1 ± 0.13	3.2 ± 0.49	2.5 ± 0.17	1.6 ± 0.05	29
Mrk 538	2799 ± 2	51 ± 1	6.8 ± 0.21	18 ± 0.33	11 ± 0.42	8.2 ± 0.58	2.6 ± 0.08	36
SDSSJ0119+1452					< 1.3		< 1.1	< 100
SDSSJ0218-0757					< 1.3		< 1.6	< 216
SDSSJ0222-0830					< 1.4		< 1.6	
SDSSJ0728+3532					< 1.2		< 0.91	< 91
SDSSJ0834+0139			< 0.62	< 1.2	< 0.92	< 1.1	< 0.52	< 26
SDSSJ0904+5136	4778 ± 2	41 ± 1	4.6 ± 0.21	4.2 ± 0.50	4.1 ± 0.28	2.9 ± 0.68	5.1 ± 0.23	196
SDSSJ0911+4636	4301 ± 4	41 ± 2	2.2 ± 0.16	1.7 ± 0.25	2.0 ± 0.31	1.4 ± 0.39	2.0 ± 0.15	133
SDSSJ0934+0014	4901 ± 1	59 ± 1	4.5 ± 0.071	8.5 ± 0.14	5.3 ± 0.59	1.6 ± 0.30	5.3 ± 0.08	78
SDSSJ0936+0106	4913 ± 8	57 ± 4	1.7 ± 0.21	< 2.3	< 0.94		2.0 ± 0.26	154
SDSSJ0943-0215	4815 ± 4	40 ± 2	2.7 ± 0.21	5.3 ± 0.63	3.1 ± 0.27	2.7 ± 0.43	3.0 ± 0.23	167
SDSSJ1118+6316	3234 ± 10	33 ± 3	0.7 ± 0.18	3.8 ± 0.66	0.8 ± 0.14	< 1.2	0.38 ± 0.094	100
SDSSJ1234+0139	4687 ± 8	59 ± 4	2.0 ± 0.24	< 2.2	2.2 ± 0.26	< 2.2	2.2 ± 0.26	147
SDSSJ1319+5203					< 1.0		< 1.1	< 100
SDSSJ1402+0955	4259 ± 4	43 ± 2	2.9 ± 0.22	4.8 ± 0.45	3.1 ± 0.25		2.6 ± 0.20	55
SDSSJ1507+5511	3366 ± 12 ^b	13 ± 3 ^b			0.5 ± 0.19		0.29 ± 0.11	69
SDSSJ2317+1400	4434 ± 2	32 ± 1	6.7 ± 0.27	13 ± 0.75	7.1 ± 0.44	4.9 ± 0.47	6.5 ± 0.26	191

^a from J=2-1 $\theta = 11''$ ^b from J=2-1 $\theta = 21''$

Table 3. CO Integrated Intensity Ratios (all $\theta = 21''$)

Source	\mathcal{R}_{21}	\mathcal{R}_{31}	\mathcal{R}_{32}
Mrk 297	0.83 ± 0.026	0.24 ± 0.033	0.29 ± 0.041
Mrk 325	1.1 ± 0.14	0.89 ± 0.068	0.78 ± 0.060
Mrk 538	1.6 ± 0.079	1.2 ± 0.093	0.75 ± 0.060
SDSSJ0904+5136	0.89 ± 0.074	0.63 ± 0.15	0.71 ± 0.17
SDSSJ0911+4636	0.91 ± 0.16	0.64 ± 0.18	0.70 ± 0.22
SDSSJ0934+0014	1.2 ± 0.13	0.36 ± 0.067	0.30 ± 0.067
SDSSJ0943–0215	1.1 ± 0.13	1.0 ± 0.18	0.87 ± 0.16
SDSSJ1118+6316	1.1 ± 0.33		
SDSSJ1234+0139	1.1 ± 0.19		
SDSSJ1402+0955	1.1 ± 0.12		
SDSSJ2317+1400	1.1 ± 0.080	0.73 ± 0.077	0.69 ± 0.080

Table 4. Inferred N_{CO} used in LVG Models

Source	N_{CO} (cm^{-2})
Mrk 297	4.5×10^{17}
Mrk 325	5.2×10^{16}
Mrk 538	1.2×10^{17}
SDSSJ0904+5136	8.3×10^{16}
SDSSJ0911+4636	3.4×10^{16}
SDSSJ0934+0014	8.1×10^{16}
SDSSJ0943–0215	4.9×10^{16}
SDSSJ2317+1400	1.2×10^{17}

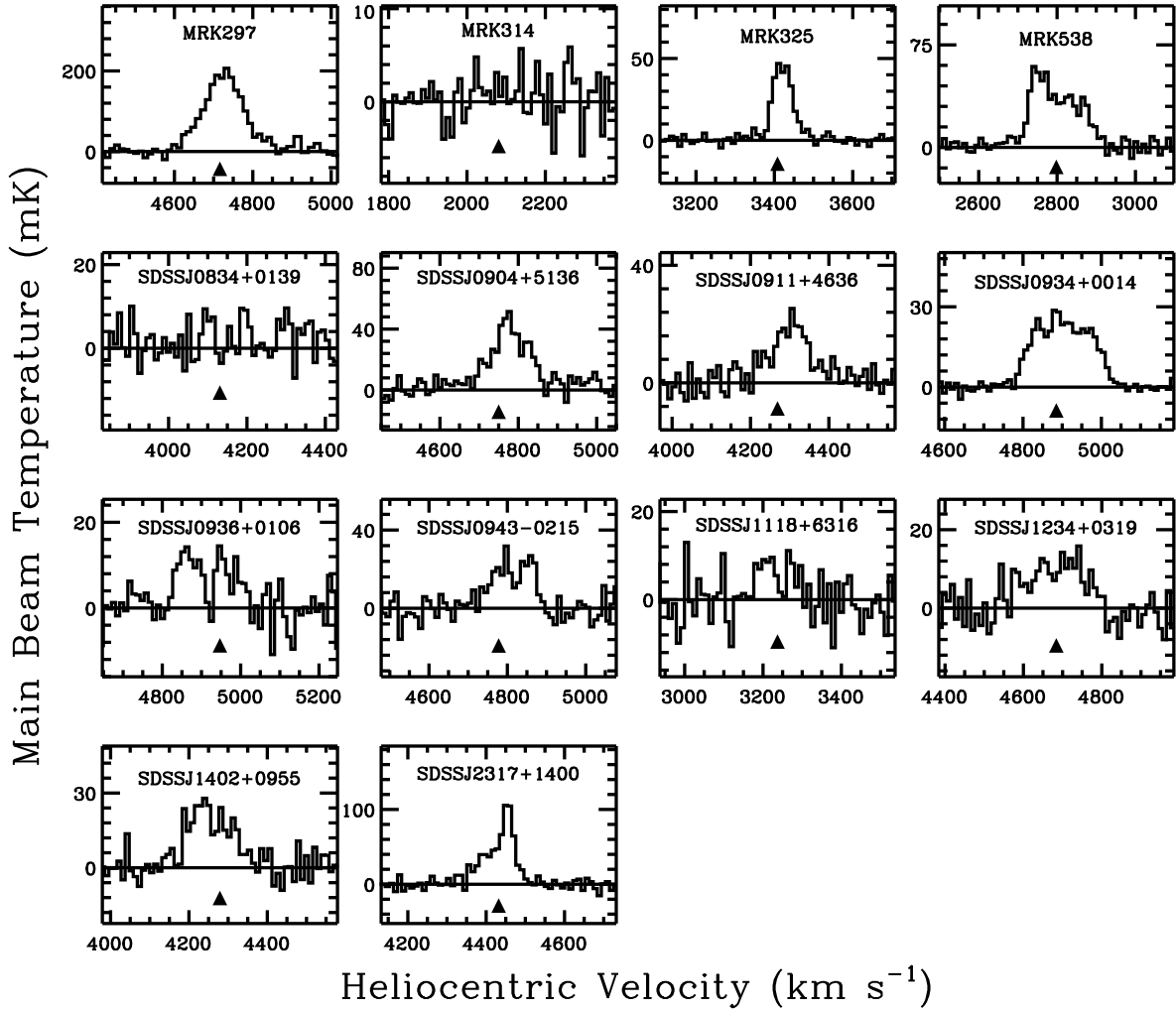


Fig. 1.— IRAM 30 m CO($J=1-0$) spectra of the sample of nearby LCBGs. The vertical scales are main beam temperatures, in mK; the horizontal scales are heliocentric velocities, in km s^{-1} . The spectra have been smoothed to a resolution of $\sim 10 \text{ km s}^{-1}$ and only the central 600 km s^{-1} are shown. The triangles indicate the recession velocities calculated from SDSS redshifts for the SDSS galaxies; velocities from NED redshifts are shown for the non-SDSS galaxies.

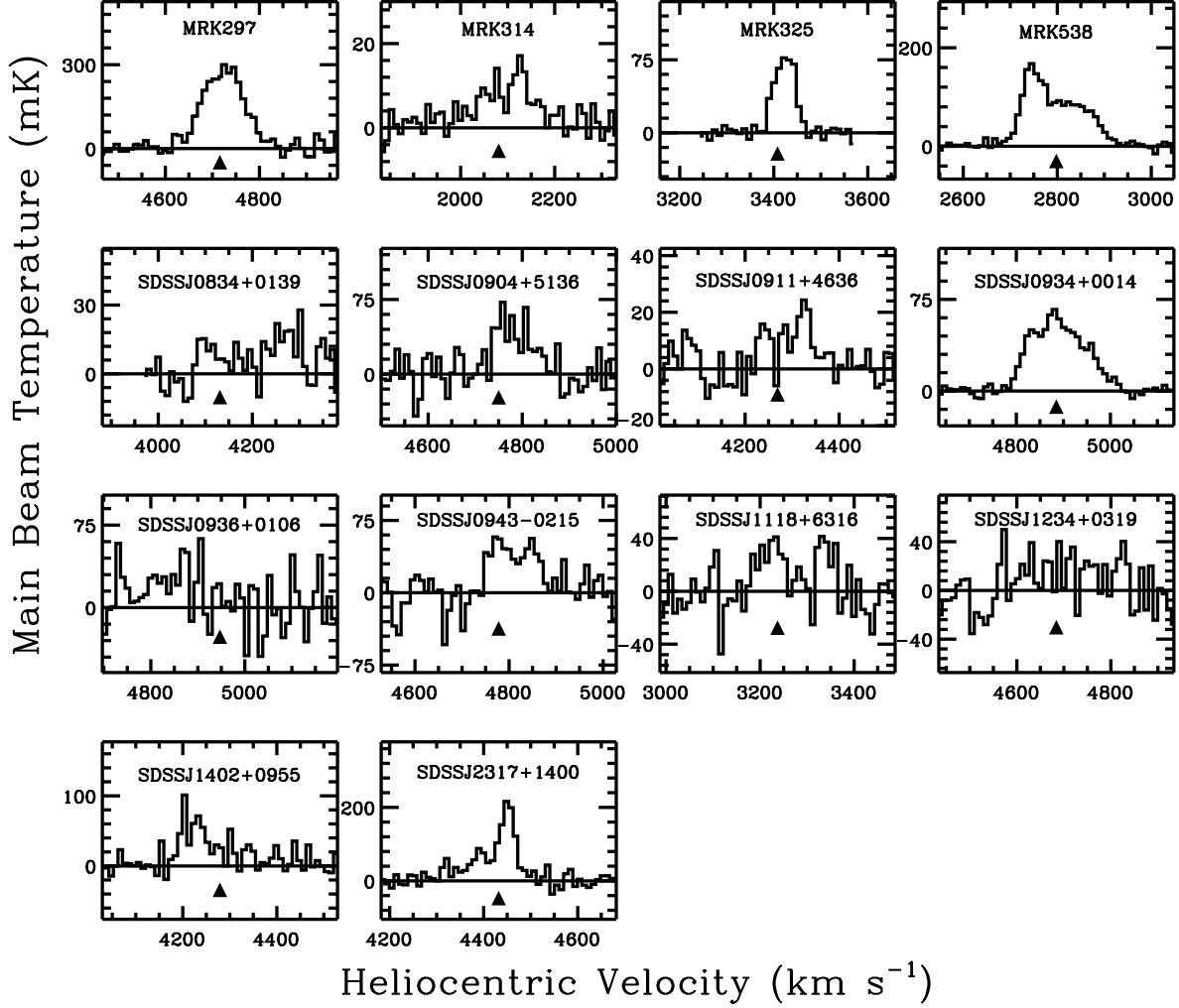


Fig. 2.— The central 500 km s⁻¹ of the IRAM 30 m CO(J=2–1) spectra of the sample of nearby LCBGs. The scales and labels are as in Figure 1. Note that these observations have a beam size half that of all others, 11''.

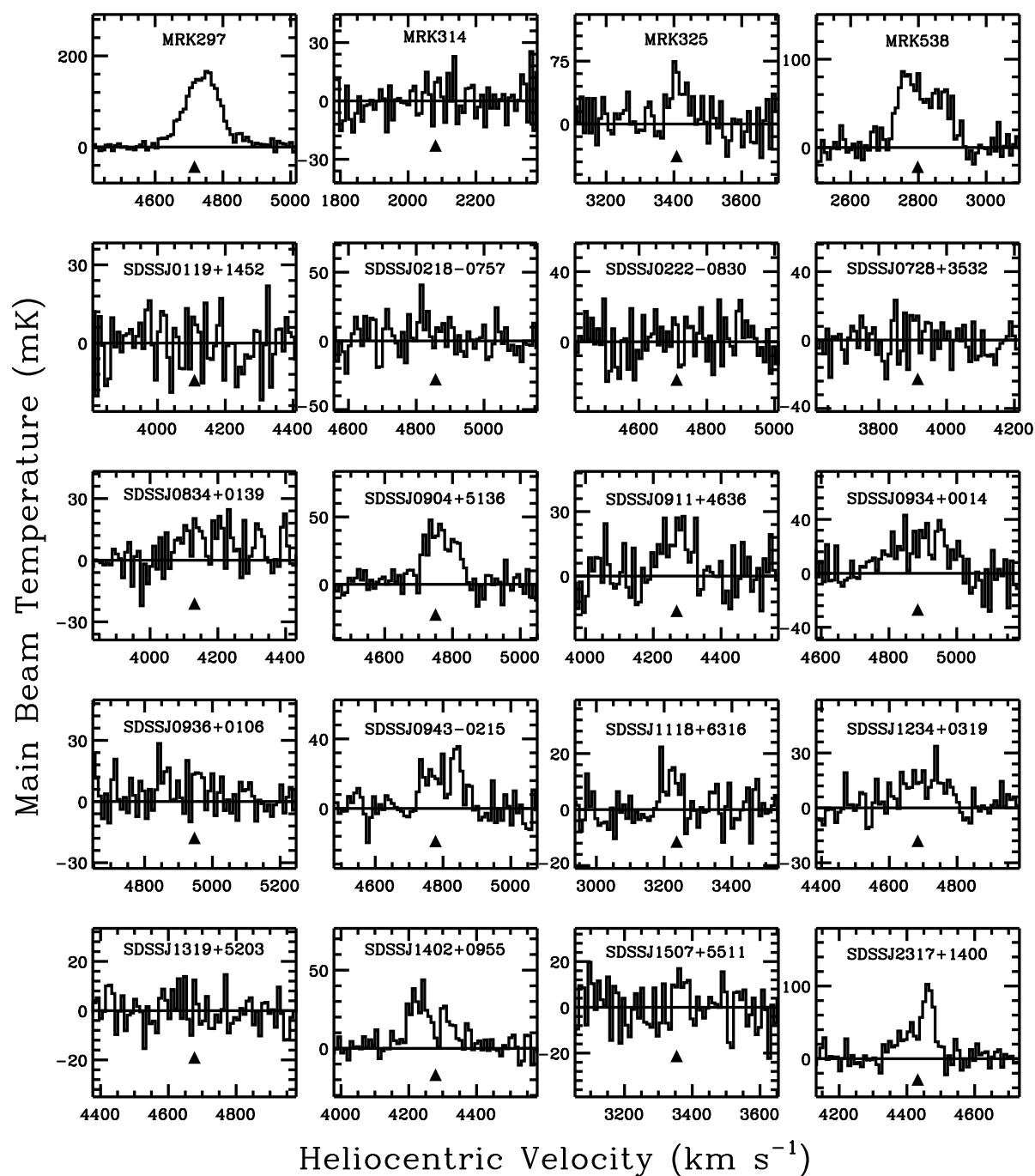


Fig. 3.— The central 600 km s^{-1} of the JCMT CO($J=2-1$) spectra of the sample of nearby LCBGs. The scales and labels are as in Figure 1.

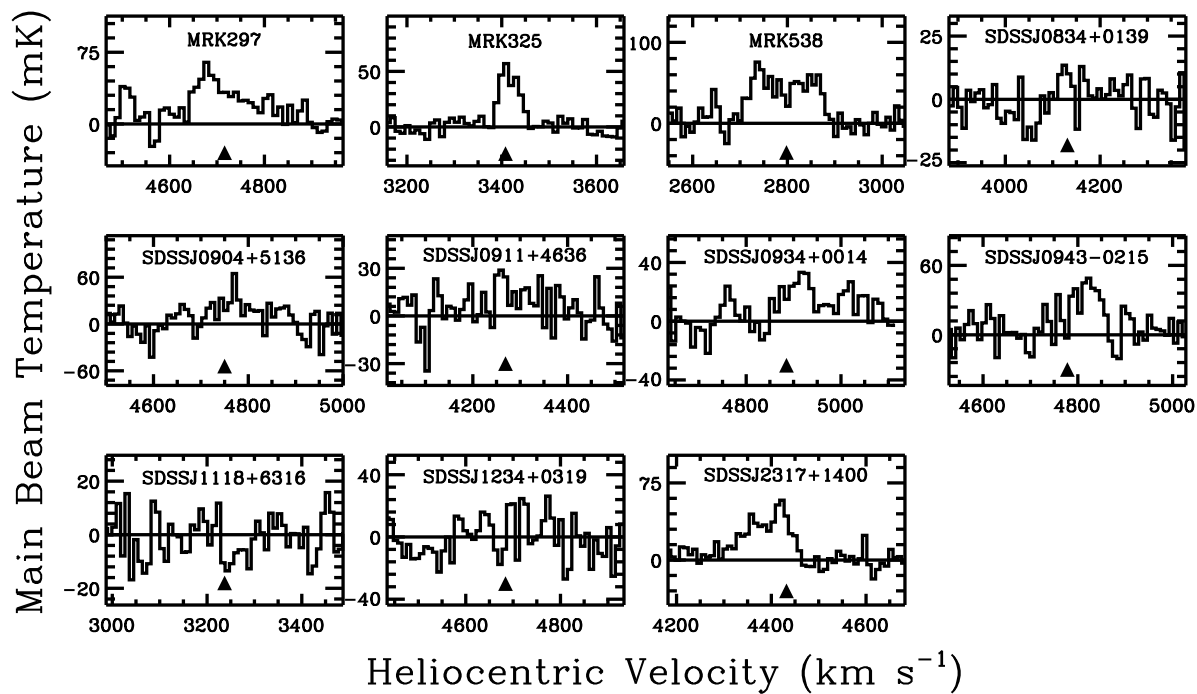


Fig. 4.— The central 500 km s^{-1} of the HHT and CSO $\text{CO}(J=3-2)$ spectra of the sample of nearby LCBGs. The scales and labels are as in Figure 1.

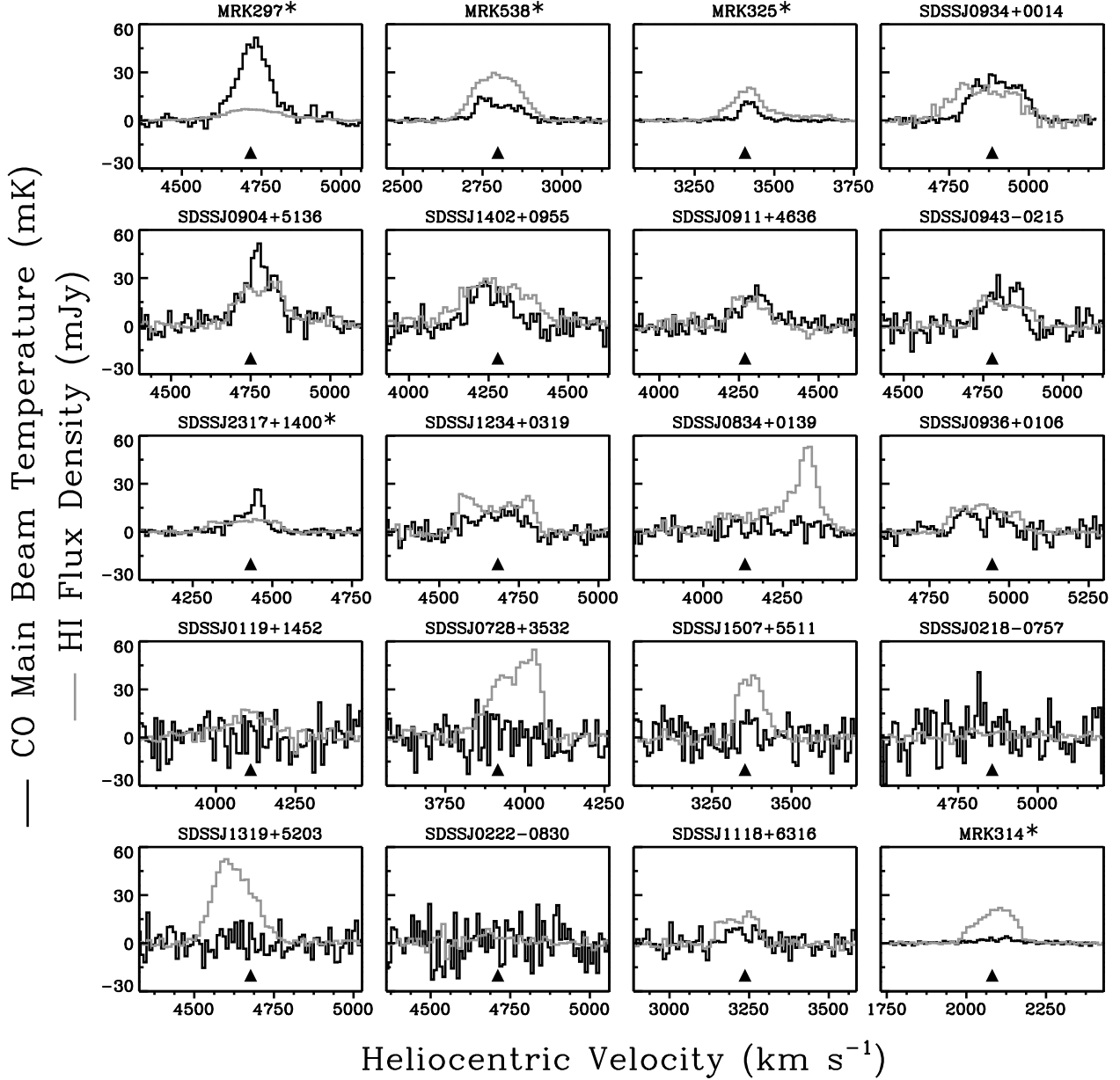


Fig. 5.— Comparison of CO and HI spectra for the 20 galaxies in our sample, ordered from brightest to faintest absolute blue magnitude. The CO spectra are shown as the darker line and either IRAM or JCMT data (see text). The gray line shows the HI spectra from Paper I and the triangle indicates the velocity of each galaxy measured from optical emission lines. All galaxies are plotted on the same temperature/flux density scale except for five galaxies, indicated by asterisks, where the spectra have been scaled down by a factor of four.

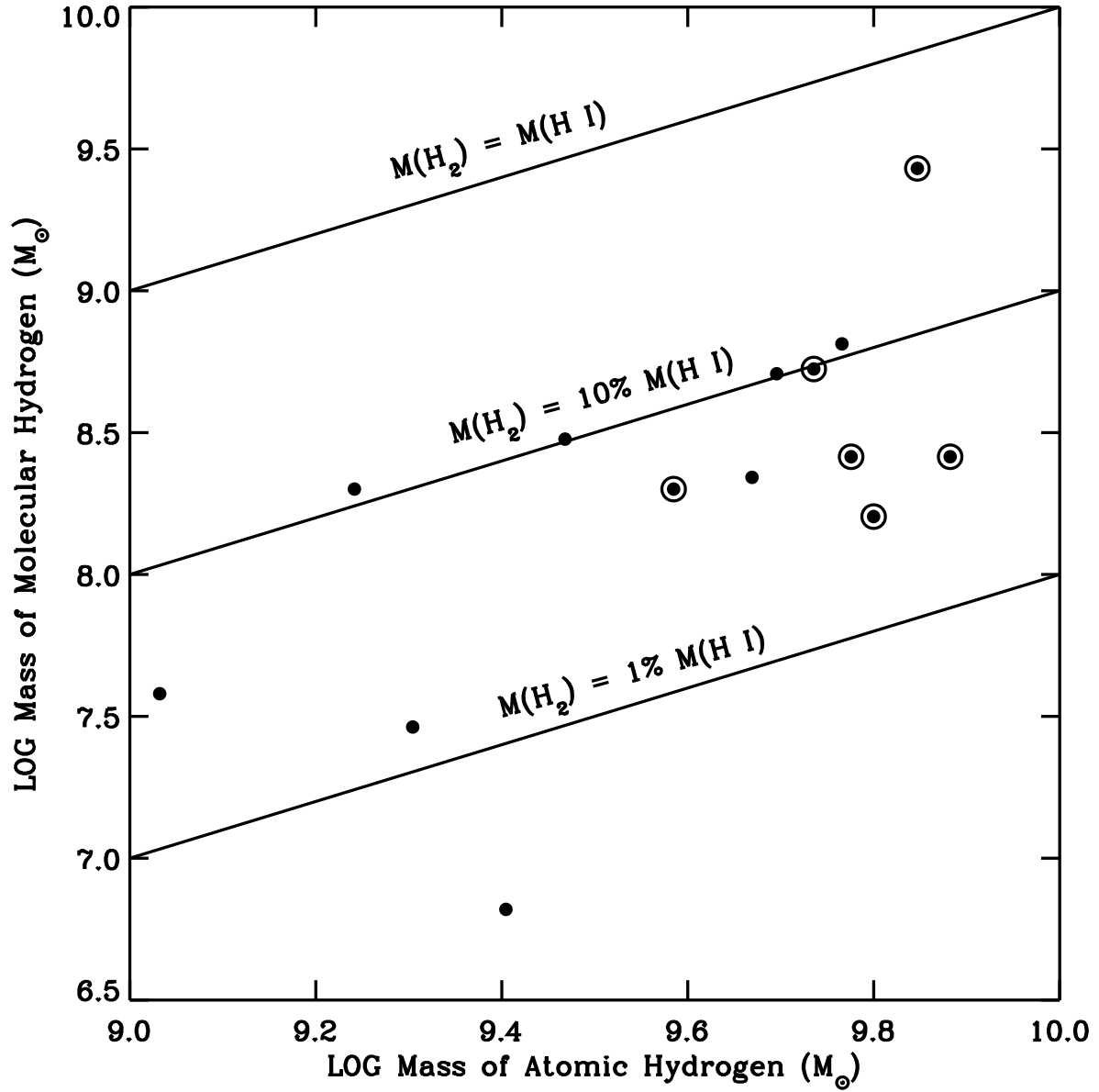


Fig. 6.— Molecular versus atomic hydrogen mass for the sample of local LCBGs. Galaxies with companions within the 9' GBT beam, for which the H I mass may be overestimated, are circled.

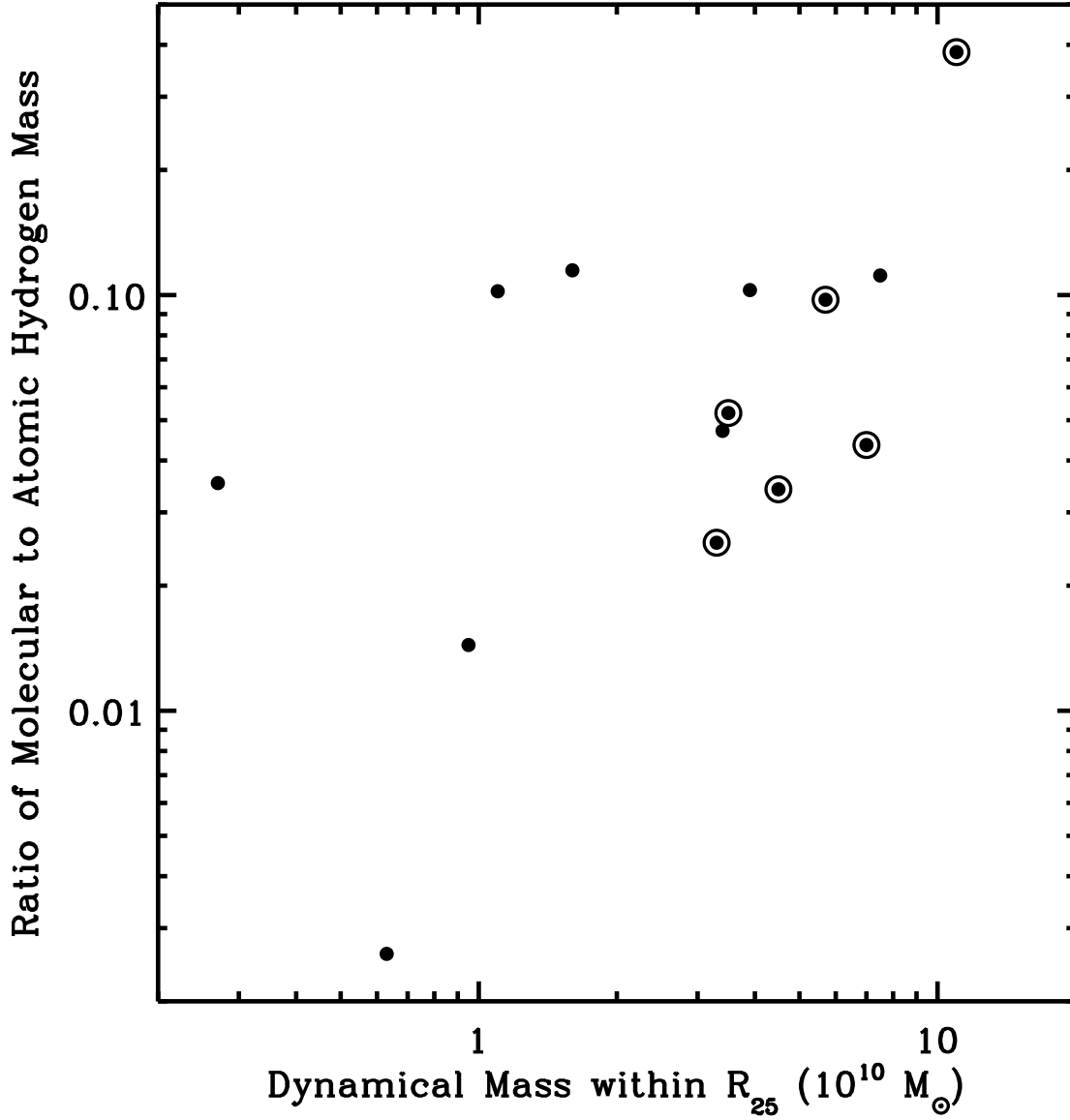


Fig. 7.— The dynamical mass (within R_{25}) is plotted versus the molecular to atomic mass fraction in local LCBGs. Circled galaxies have companions within the 9' GBT beam and may have slightly overestimated H I masses. Nevertheless, there is a slight overall trend for the fraction of molecular hydrogen to increase with increasing dynamical mass.

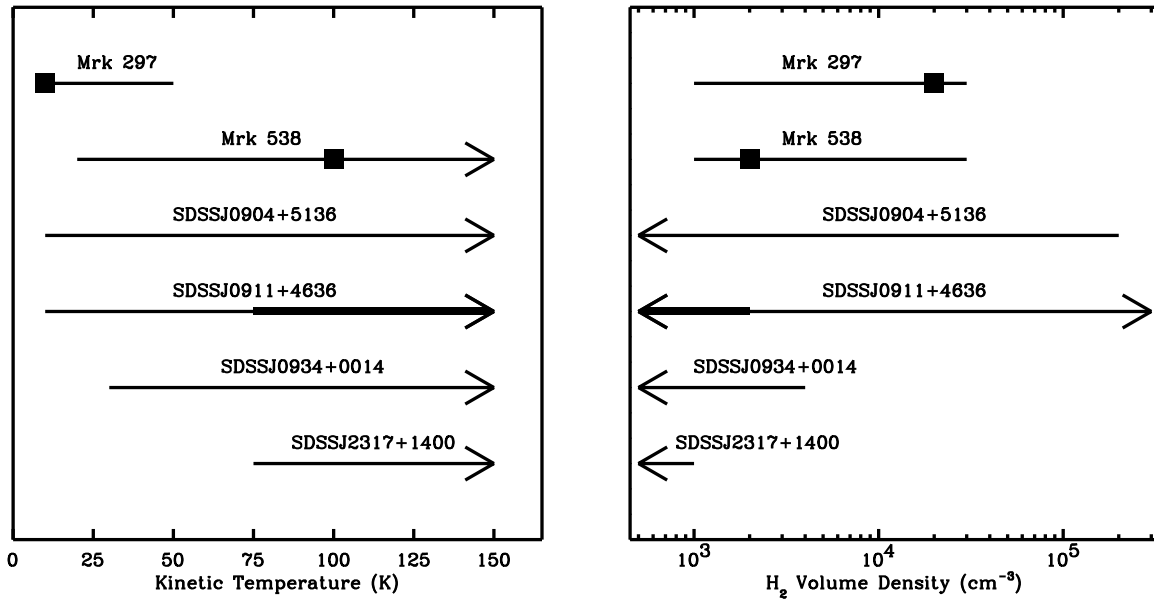


Fig. 8.— The ranges of possible kinetic temperatures (left) and molecular hydrogen volume densities (right) for local LCBGs as predicted by LVG modeling. Model fits to within $\pm 3\sigma$ of the observed values are indicated by thin lines/arrows, while those to within $\pm 1\sigma$ are indicated by heavy lines or dark rectangles (where only one solution was found in the model grid).

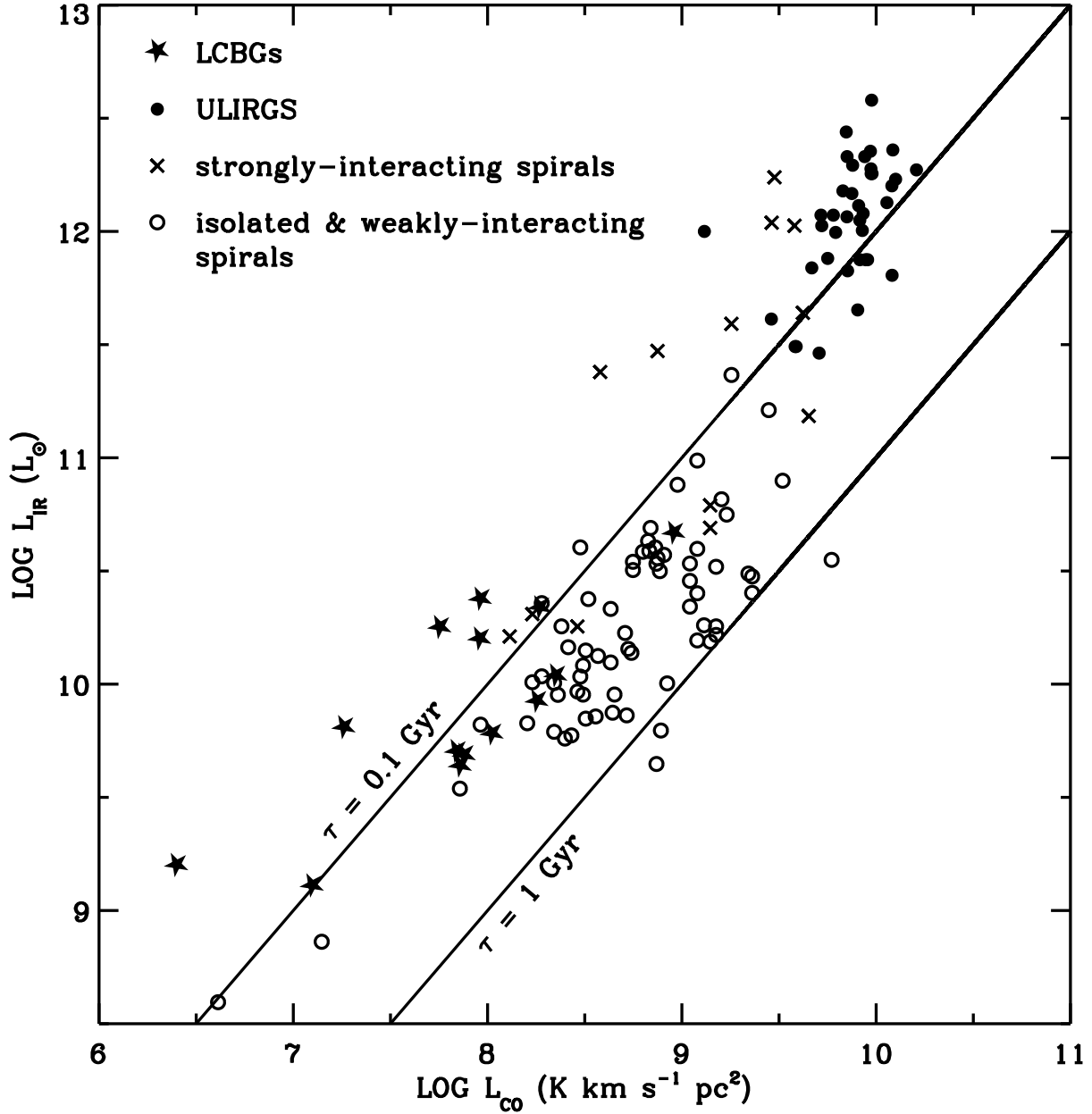


Fig. 9.— Infrared versus CO luminosities for local LCBGs (stars) and other galaxy types: isolated or weakly-interacting local spirals (open circles), strongly-interacting local spirals (×’s), and UltraLuminous InfraRed Galaxies (ULIRGs, filled circles) (Solomon et al. 1997; Solomon & Sage 1988). Lines indicating gas depletion time scales of 10^8 and 10^9 years are indicated. LCBGs have short gas depletion time scales, similar to ULIRGs and strongly-interacting local spirals.

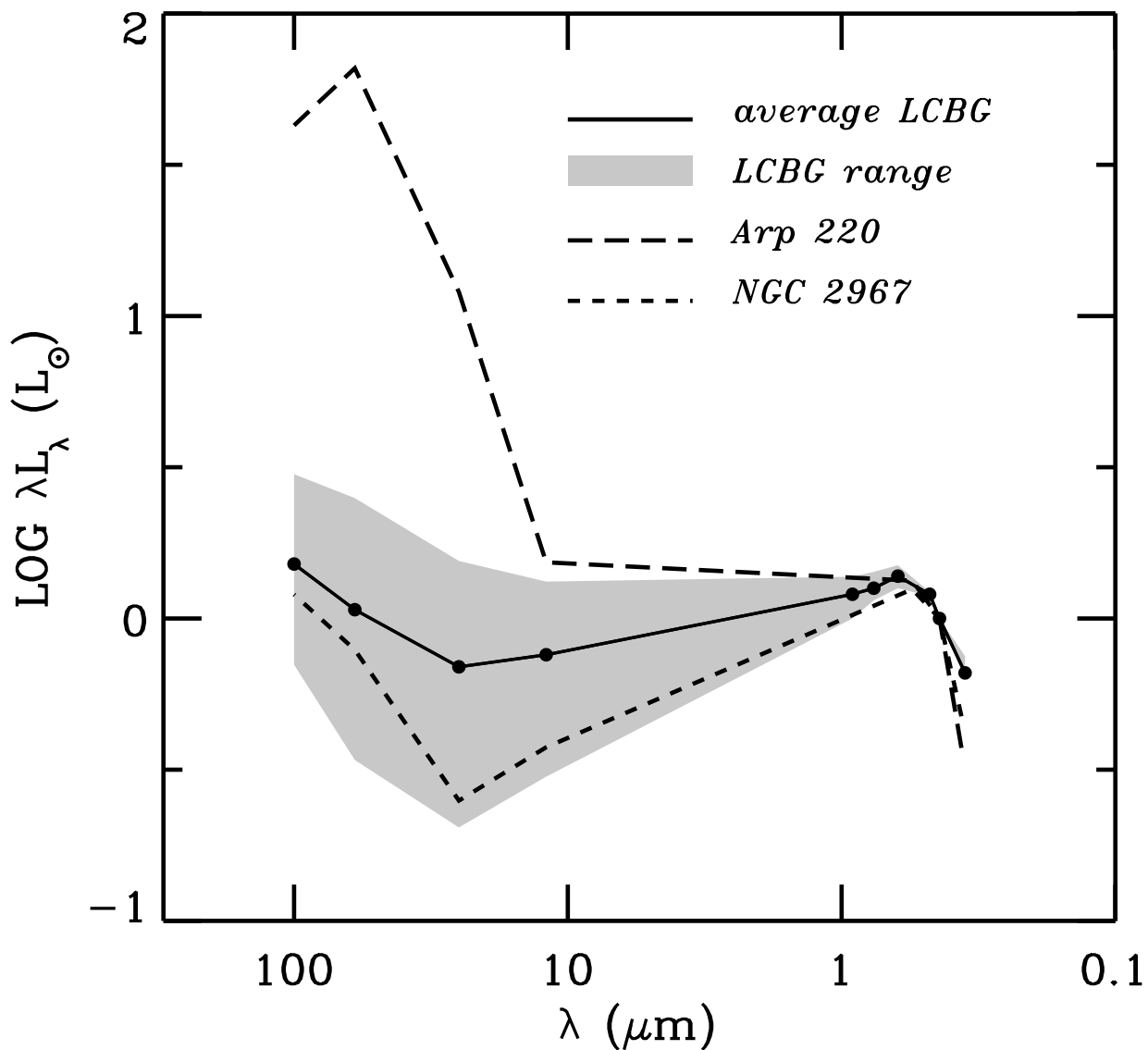


Fig. 10.— Spectral energy distribution of LCBGs in comparison with a normal spiral galaxy, NGC 2967, and a luminous infrared galaxy, Arp 220. Optical fluxes were derived from the SDSS or NED where appropriate. The far-infrared fluxes are from IRAS. The average for the local LCBG sample is shown by the solid line and the range by the gray area. For comparison, each SED is normalized to the B-band value.